Moroccan Journal of Chemistry
ISSN : 2351-812X

Mor. J. Chem., 2023, Volume 11, Issue 01, Page 205-220
https://revues.imist.ma/index.php/morjchem

Molecular design of D-π-A-π-D conjugated molecules based on carbazole for application in solar cells

Khaddam Y.[1]*, Kacimi R.[1], Azaid A.[1], Bouachrine M.[1,2], Maghat H.[1]**
[1]*Molecular Chemistry and Natural Substances Laboratory, Faculty of Science, University Moulay Ismail, Meknes, Morocco*
[2]*EST Khenifra, Sultane Moulay Slimane University, Khenifra, Morocco Chemistry and Natural Substances Laboratory, Faculty of Sciences, University Moulay Ismail, Meknes, Morocco*
**Corresponding author, Email address: khaddamyns@gmail.com*
***Corresponding author, Email address: h.maghat@umi.ac.ma*

Received *14 Oct 2022,*
Revised *15 Jan 2023,*
Accepted *17 Jan 2023*

Citation*: Khaddam Y., Kacimi R., Azaid A., Bouachrine M., Maghat H. (2023) Molecular design of D-π-A-π-D conjugated molecules based on carbazole for application in solar cells, Mor. J. Chem., 14(1), 205-220. Doi: https://doi.org/10.48317/IMIST.PRSM/morjchem-v11i1.37306*

Abstract: In order to obtain molecules with D-π-A-π-D (donor-π-acceptor-π-donor) architecture, having a high performances photovoltaic effect for the recommended for chemical synthesis for use in the field of organic solar cells. We took the M1 (Kadam *et al*., 2020) as a reference symbolized in this work by R; the acceptor unit A is replaced by other acceptors, the aim was to explore the efficient organic molecule by investigating the electronic, photovoltaic and optical properties. All calculations were done on Gaussian 09 software, the optimization of the structures of studied molecules, the calculation of HOMO - LUMO energies and the energy gap was carried out by density functional theory (DFT) at B3LYP/6-31G (d) functional. The vertical electronic excitation was determined using time dependent DFT (TD-DFT) at selected hybrid CAM-B3LYP functional. The aim was to find molecules wavelengths, the results established and the properties obtained show the importance of these molecules in the photovoltaic field.

Keywords: DFT; TD-DFT; LUMO; HOMO; B3LYP; CAM-B3LYP; donor; acceptor.

1. Introduction

Nowadays, the energy is a critical factor in social and economic progress. However, the extensive use of fossil fuels product in greenhouse gases, such as carbon dioxide, causing global warming, ozone depletion, and natural disasters (Bibi *et al*., 2021). The scarcity of fossil fuels, global warming and the increase growing energy demands are factors favored the emergence of renewable energies as an alternative to classical sources. Researchers have considered biomass, solar, geothermal, ocean, wind, hydropower and liquid biofuels as sources of clean and renewable energies that are replacing conventional fossil fuels, to challenge for sustainable development. Solar energy is a promising candidate in solving these environmental issues without replenishing adverse effects. in looking for solar energy sources, organic photovoltaic technologies is one of the most important and promising long-term strategies for providing clean, low-cost and inexhaustible energy to our planet (Chen, 2016).

Silicon is, by far the most widely semiconductor material used in the field of photovoltaic cell. Nevertheless, due to the expensive cost of silicon solar cells and their complicated manufacturing

process, scientists have recently been developed alternative solar cell technologies using organic Photovoltaic("Photovoltaics - CSIRO" n.d.). Lightness, flexibility, low-cost manufacturing (Gambhir *et al.,* 2016), environmentally friendly (Burke and Lipomi, 2013) and easy fabrication (Günes *et al*., 2007) are the benefits of using organic photovoltaic for the production of solar cells.

Currently, bulk heterojunction (BHJ) and dye-sensitized solar cell (DSSC) considered as reliable technologies photovoltaic that complement silicon cell. These new compounds characterized by an alternation of σ and π bond, which results in a high mobility of intermolecular charge and their reports of appreciable conductivities. These small conjugated molecules have a well-defined molecular framework with the flexibility to modify properties through structural modification (Kadam et al. 2020). Scientists have recently produced a new materials by combination of carbazole material with a variety of conjugated units (Britel *et al*., 2022; Grazulevicius *et al*., 2003). These Carbazole derivatives are potential organic compounds used in optoelectronic applications, such as organic light emitting diodes (OLEDs) (Ledwon, 2019), organic field effect transistors (OFETs) (Souharce *et al.*, 2009), electrochromic devices (ECDs) (Aydin and Kaya, 2013), bulk heterojunction solar cells (BHJ) (Sathiyan *et al*., 2018) and dye-sensitized solar cells (DSSC) (Duvva *et al*., 2015). Small carbazole molecules are of interest as optoelectronic photoconductors or charge transporting materials due to following raisons (Grazulevicius *et al*., 2003; Ates and Uludag, 2016):

- Wide range of functionalization options, as well as chemical and environmental stability;
- HOMO and LUMO energy levels that are predictable (easily adjusted by chemical substitution);
- Carbazoles form a stable radical cation very quickly;
- The charge carrier mobilities of some carbazole compounds are quite high;
- The carbazole ring can simply be modified with different substituents;
- Carbazole containing compounds are thermally and photochemically stable;
- Carbazole is a low-cost raw material easily derived from coal tar distillation.

Using the carbazole as donor and Dithienopyrrolobenzothiadiazole (DTPBT) as acceptor units, Kadam and co-workers have been synthesized a new D-π-A-π-D type macromolecule. Spectroscopic techniques and DFT calculations were used to investigate the optoelectronic properties of this new compound. In present study, four D-π-A-π-D conjugated molecules (M1-M4) are designed to find their opto-electronic properties. These molecules are obtained by substitution of the acceptor unit of the compound already synthetized (R) by four other units to improve their electronic, optical and photovoltaic properties, in order to search for new molecules with a photovoltaic performance for use in the field of organic solar cells (Idrissi *et al.,* 2020).

2. Computational details

In order to find the best electronic and photovoltaic properties, we took the molecule M1 that already synthetized by Vinay S. Kadam as a reference (R), and we replaced the Dithienopyrrolobenzothiadiazole by four other acceptors (**Figure 1**). All calculations have been found by Gaussian 09 package (Vincenzo *et al*., 2013) and the visualization was carried out using GaussView 6.0 program. We used the density theory (DFT) with the function of the three Becke parameters and the function of Lee Yang-Parr (B3LYP) (Bauschlicher and Partridge, 1995) related to 6-31G (d) (Becke, 1993) for optimize the geometry of molecules in the ground state, and also to calculate the HOMO - LUMO energy levels and the gap energies for all molecules. This study includes the predicting of the Voc open circuit voltage and αi parameter of electronic injection. The optical properties of the organic molecules, the absorption maximum (λmax) and the oscillator forces (OS) or optical transitions are

found using density-time functional theory (TD-DFT) (Ates and Uludag, 2016). The 6-31G (d) basis set is used for all calculations (Sadiki et al., 2015; Khlaifia *et al.,* 2020). To choose the appropriate functional to describe the effects of excitation, we have plotted the ultraviolet absorption spectrum of the reference R by four different functional B3LYP, CAM-B3LYP, MPW1PW91 and WB97XD in order to select the best functional having in accordance to the experimental value. The functional reproduced the best results will be using by which we will treat the molecules studied.

The electronic properties of conjugated organic compounds are intimately linked at the gap energy (Belghiti, 2017). The gap energy is evaluated as a difference between the HOMO and LUMO levels with the following equation:

$$E_{gap} = E_{LUMO} - E_{HOMO} \qquad \textbf{Eqn 1}$$

The yield of photovoltaic cell is proportional on the open circuit voltage Voc. The theoretical value of the Voc can be calculated from the following equation:

$$Voc = \frac{1}{e}\left(\left|E^{D}_{HOMO}\right| - \left|E^{A}_{LUMO}\right| - 0,3\right) \qquad \textbf{Eqn 2}$$

Where E^{D}_{HOMO} and E^{A}_{LUMO} are respectively the energy levels of HOMO of donor and LUMO of acceptor, 0,3 is an empirical value for efficient charge separation (Duan *et al*., 2013).

For a possible efficient electron transfer from the molecule Mi (donor) to PCBM (acceptor), another parameter noted αi was examined, it is the difference between the LUMO energy levels of the studied compounds and the LUMO energy levels of PCBM (El Alamy *et al*., 2015).

$$\alpha i = E_{LUMO}\left(Mi = 1-4\right) - E_{LUMO}(PCBM) \qquad \textbf{Eqn 3}$$

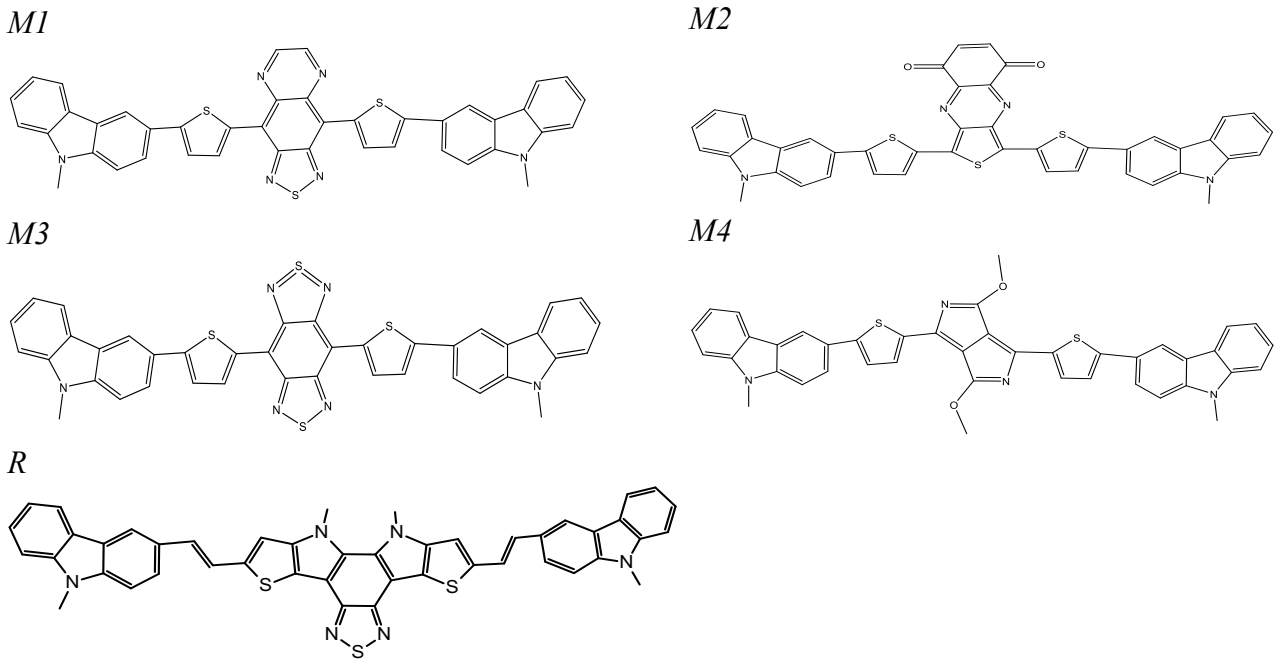

Figure 1. Structural representation of all the molecules (M1-M4 and R) using Chem Draw Ultra 12.0

3. Results and Discussion

3.1 Organic compounds optimization

3.1.1 Geometries optimization

All the structures obtained by B3LYP/6-31G (d) (**Figure 2**) have a quasi-planar conformation, indicating that the modification of the acceptor group does not affect the geometric parameters.

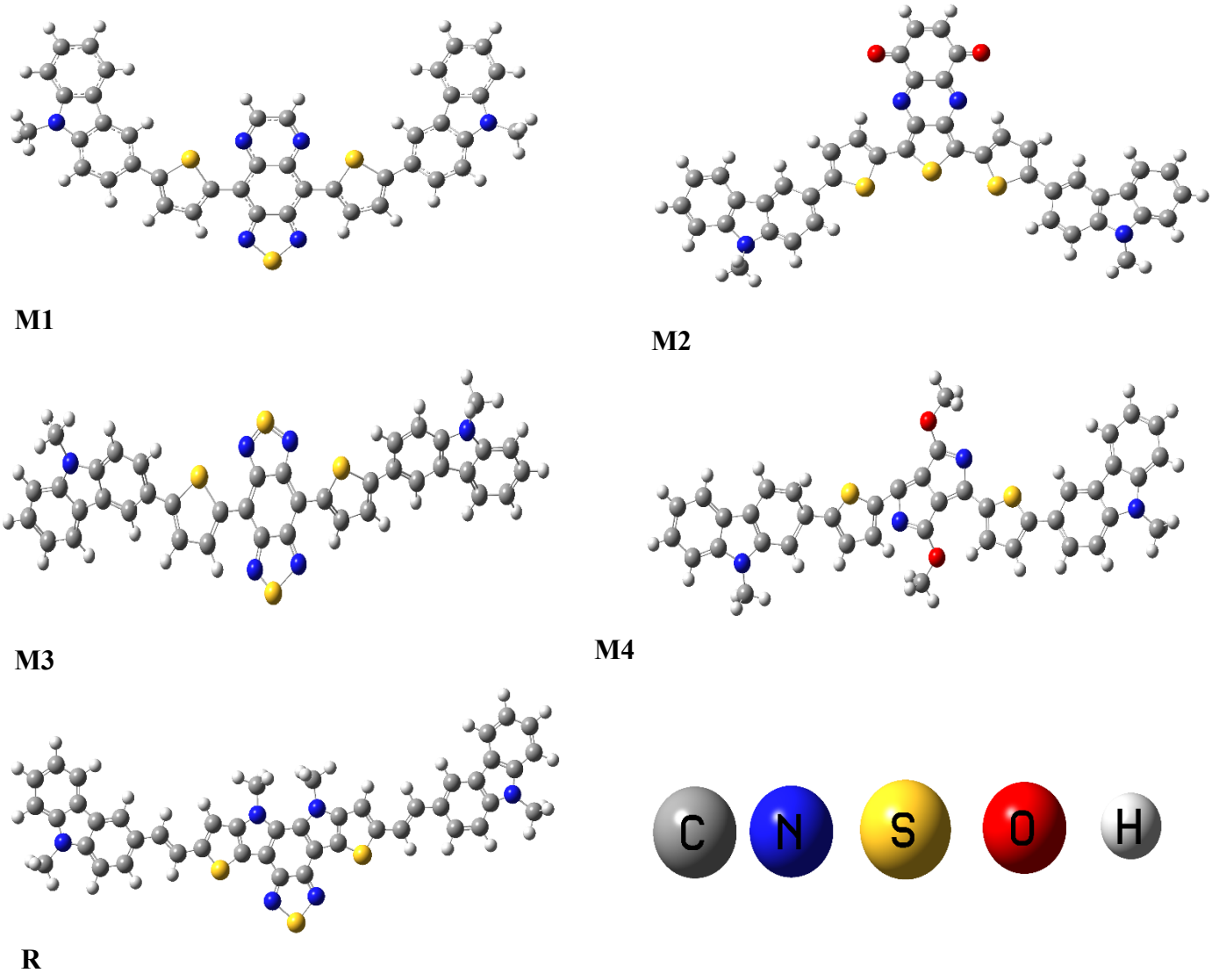

Figure 1. Optimized geometries obtained by B3LYP /6-31G(d) of studied molecules (M1-M4 and R)

3.1.2 Electronic and photovoltaic properties of the proposed donors

In **Tables 1** and **2**, we presented respectively the electronic and photovoltaic properties of all molecules in their isolated state and in chloroform solvent. As shown in **Table 1**, the modification of the molecular structure affects the HOMO and LUMO levels. The trend of HOMO energies was M2<M4<M1<M3<R while for the trend of LUMO energies was M3<M1<M2<M4<R and the trend of gap energies was M3(1.23) <M1(1.49) <M2(1.73) <M4(2.10) <R (2,55). The gap energy obtained for the four proposed molecules is much better than the one of reference. The energy difference (noted αi) between LUMO level of each compound (Mi,i=1-4), and LUMO level of the PCBM, (acceptor compound) varies from 0.44 to 1.17; these values indicate that the electron transfer from studied molecules to the PCBM, may be sufficiently efficient in photovoltaic devices.

Table 1: HOMO energies (EHOMO), LUMO energies (ELUMO) and gaps (Eg) of all molecules in the gas phase obtained by B3LYP /6-31G(d) level.

Compounds	E_{HOMO} (ev)	E_{LUMO} (ev)	Egap	Voc (V)	Alpha
M1	-4.54	-3.06	1.49	0.54	0.65
M2	-4.69	-2.95	1.73	0.69	0.75
M3	-4.49	-3.26	1.23	0.49	0.44
M4	-4.62	-2.53	2.09	0.62	1.17
R	-4.37	-1.82	2.55	0.37	1.89

Table 2: HOMO energies (EHOMO), LUMO energies (ELUMO) and gaps (Eg) of all molecules in chloroform (solvent) obtained by B3LYP l6-31G(d) level.

Compounds	E_{HOMO} (ev)	E_{LUMO} (ev)	Egap	Voc	Alpha
M1	-4.73	-3.20	1.53	0.73	0.50
M2	-4.80	-3.17	1.63	0.80	0.53
M3	-4.65	-3.42	1.23	0.65	0.30
M4	-4.78	-2.77	2.02	0.78	0.94
R	-4.50	-2.00	2.50	0.50	1.70

The open circuit voltage values obtained from the studied molecules vary from 0.38 to 0.69 in the sequence R <M3 <M1 <M4 <M2. The four compounds' Voc are significantly higher than the reference molecules. In chloroform (solvent) (**Table 2**), the values of HOMO and LUMO levels were lightly changed, to alter the parameters Egap, Voc and alpha. The solvent affects the stability of the molecule, which influences his energy gap. The trend of gap energies was M3(1.23) <M1(1.53) <M2(1.63) <M4(2.02) <R (2.50). The variation observed due to their interaction between solvent and compound. The compounds (Mi,i=1-4) may be envisaged as organics active in photovoltaic devices.

3.1.3 Frontier molecular orbitals (FMOs) diagram.

The diagram is a tool, which makes it possible to compare the donor effect, the acceptor effect and the gap energy of different compounds as well as to predict the possibility of injection of the electrons of the donor molecules towards the chosen acceptor (the PCBM). The optoelectronic properties depend essentially on the appropriate HOMO and LUMO energy levels and the electron and hole mobilities (Belghiti, 2017; Duan *et al*., 2013).

3.2 molecular electrostatic potential

In this part, we have computed the molecular electrostatic potential (MEP) an important parameter for predicating the reactive nucleophilic and electrophilic attack sites of designed molecules, as well as the interactions of hydrogen bonding (Politzer and Murray, 1991). MEP at a point in the space when molecule is present provides information on the net electrostatic effect created at that point through total charge distribution (electron and nuclei) of the molecule (Thul *et al.,* 2010). MEPs have been calculated using the density functional theory at B3LYP level at 6-31G (d) basis. Different colors represent different values of the electrostatic potential at the surface; red represents regions of most negative electrostatic potential (electron-rich) and blue represents regions of most positive electrostatic potential (electron-poor) while green represents regions of zero potential.

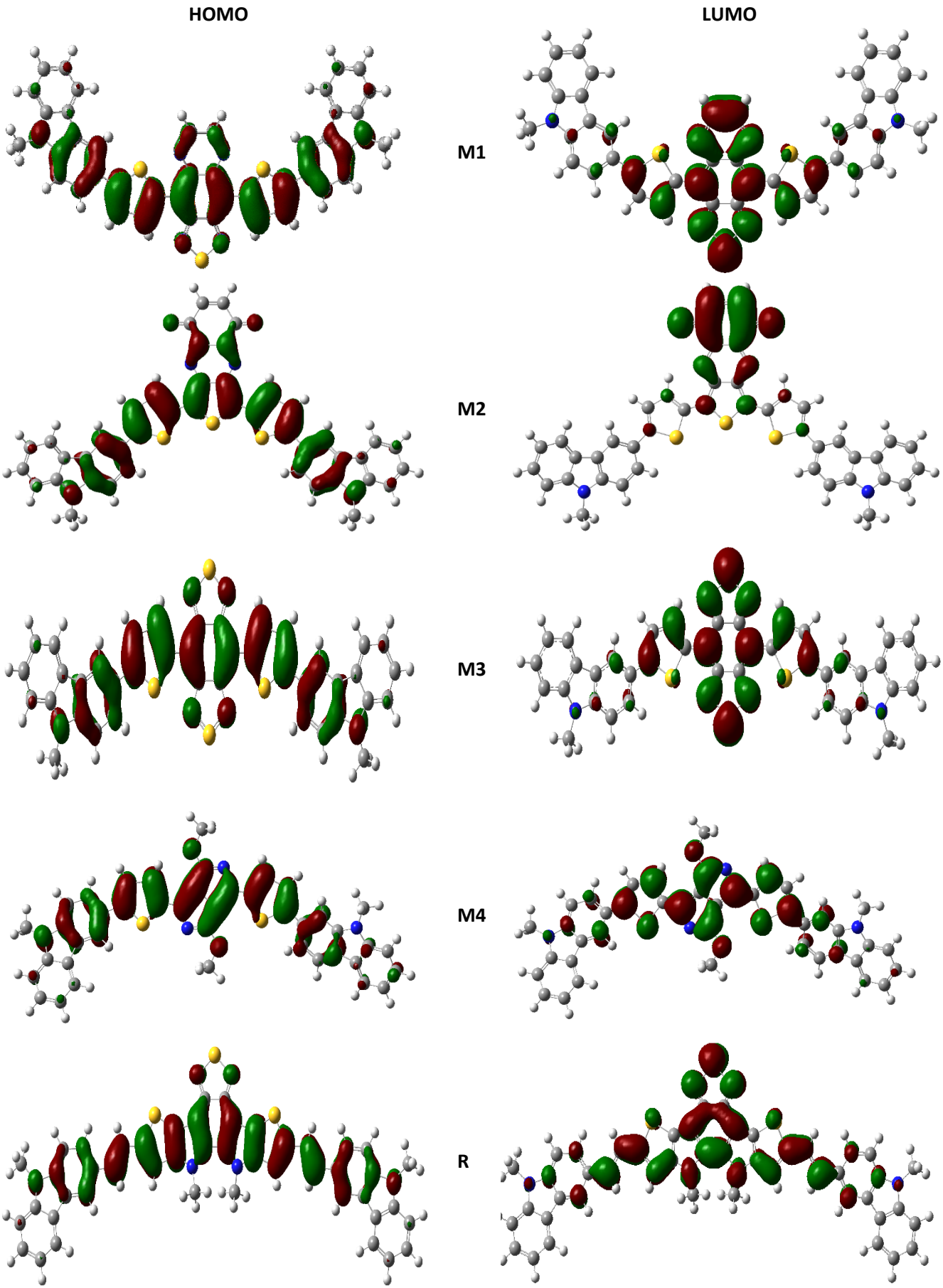

Figure 2. DFT calculated of the optimized structure all molecules (M1, M2, M3 and M4) and R, highest molecular orbital (HOMO), and lowest unoccupied orbital (LUMO).

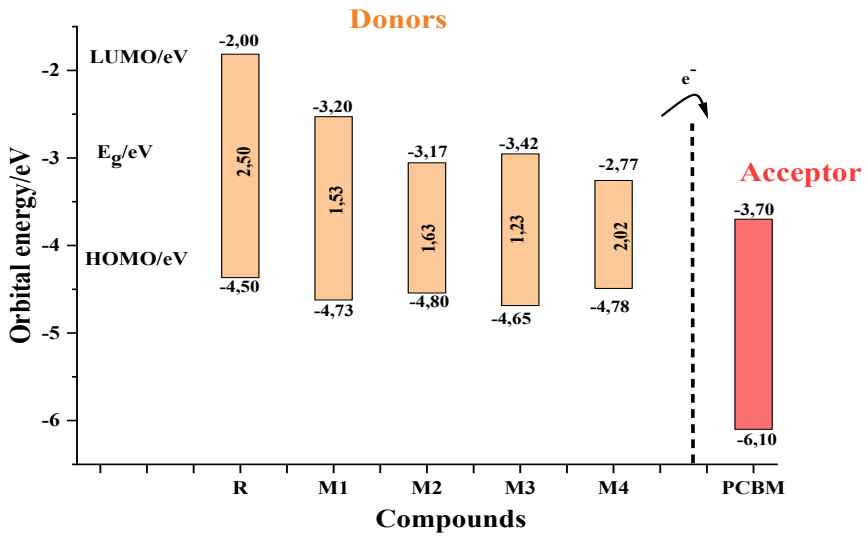

Figure 3. Energy band gaps diagram of molecules (M1-M4) and R in the gas phase

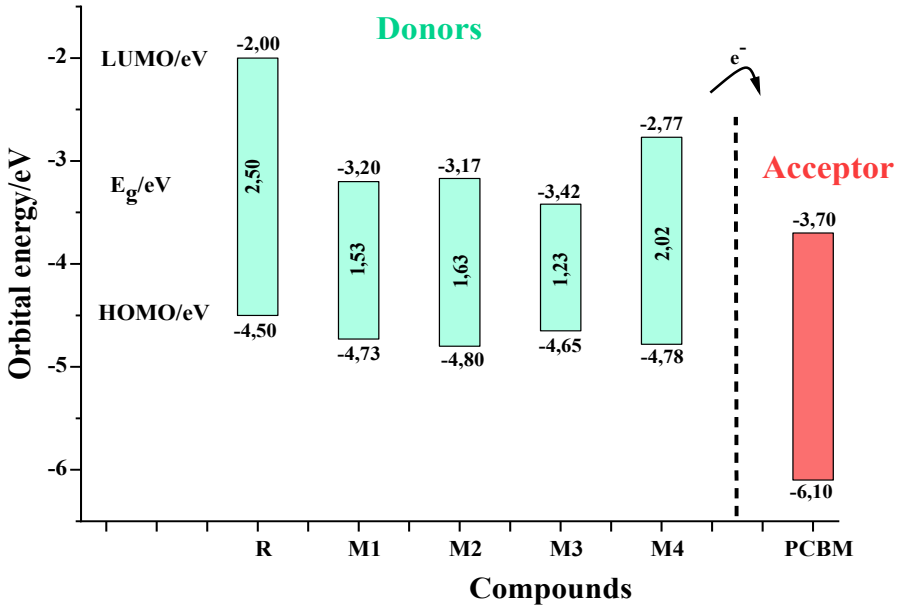

Figure 4. Energy band gaps diagram of molecules (M1-M4) and R in chloroform solvent

The investigated molecule has possible sites for electrophilic (the electrophilic sites are most electronegative) and nucleophilic attack (the nucleophilic sites are most positive) (R. Vasanthakumari *et al.*, 2018). Electrostatic potential surfaces for all compounds (Mi, i=1-4 and R) have been plotted using DFT/B3LYP/6-31G (d) (**Figure 6**). This figure highlights the different chemically active sites and reactivity of atoms.

The code of the map is in the range between a negative value (deepest red) and a positive value (deepest blue) (Wu *et al.*, 2019), (**Table 3**).

Table 3. Values of deepest red and deepest blue for proposed molecules (M1- M4) and reference R.

Compound	M1	M2	M3	M4	R
Value of deepest red	$-3.099e^{-2}$	$-5.164e^{-2}$	$-3.309e^{-2}$	$-4.531e^{-2}$	$-4.998e^{-2}$
Value of deepest blue	$3.099e^{-2}$	$5.164e^{-2}$	$3.309e^{-2}$	$4.531e^{-2}$	$4.998e^{-2}$

It is clear that the hydrogen atoms of the carbazole group represent electropositive sites while the negative potential is mainly localized on the core of the molecule M1 in particular on thiophene group and respectively on the thieno [3,4-b]quinoxaline-5,8-dione, the 1,2,5-thiadiazole and the 2-methoxy-3H-pyrrole groups of the molecules M2,M3 and M4.

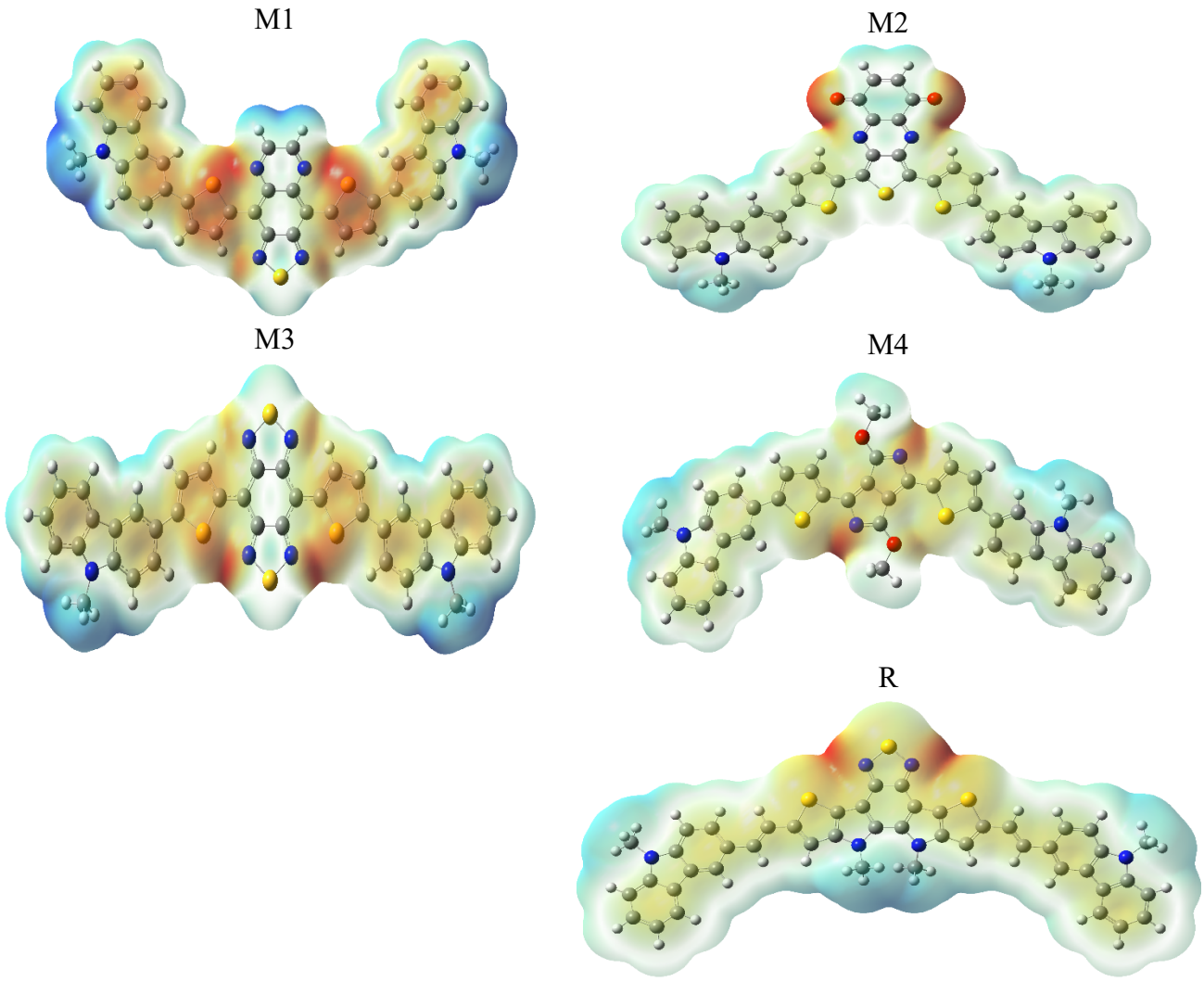

Figure. 5. Electrostatic surface potential of total electron density for all molecules (M1-M4) and R obtained by B3LYP l6-31G(d) level. Regions of higher electron density are shown in red and of lower electron density in blue

3.3 absorption properties

3.3.1 Choose of method

To choose the appropriate functional to describe the effects of excitation, we conducted several tests with different functional (B3LYP, CAM-B3LYP, MPW1PW91 and WB97XD) on the reference compound R. The absorption spectra of the reference molecule obtained by different functionals is represented in the **Figure 7** and the λ_{max} values obtained from these four functionals were compared with the experimental value in **Figure 8**. We remark that the value of the absorption length (λ_{max}) obtained by functional CAM-B3LYP with basis set 6-31G(d) for the reference molecule is agree with this obtained experimentally as compared to other functional (B3LYP, MPW1PW91 and WB97XD), this indicates that the functional CAM-B3LYP is appropriate to describe the effects of excitation a long range. Thus, in this work, we will use the functional CAM-B3LYP to predate the properties of absorption of compounds (Mi, i=1-4) proposed.

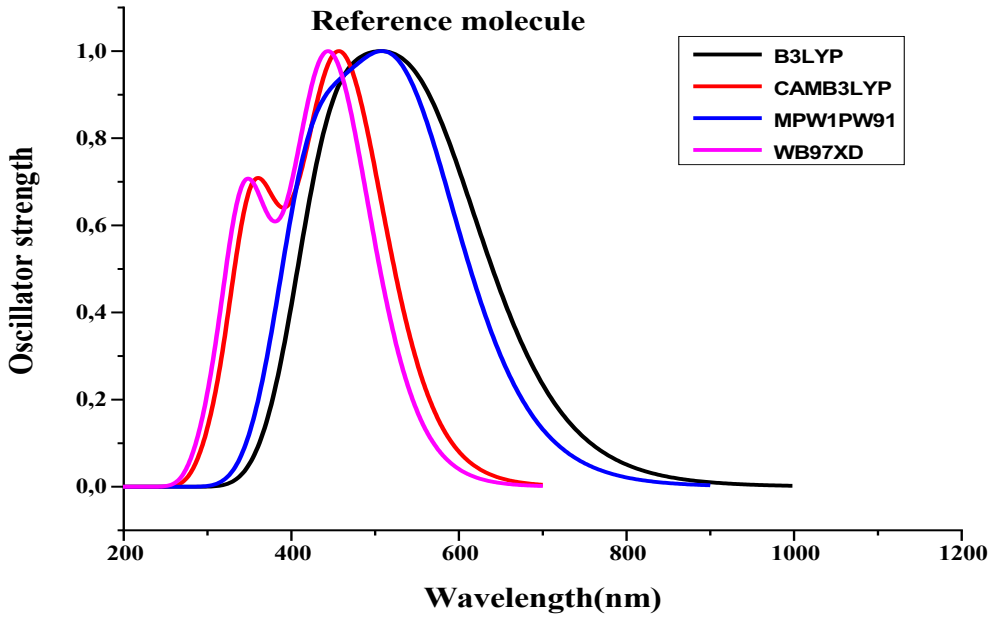

Figure 6. Absorption profile of R molecule calculated at four dissimilar hybrid functional

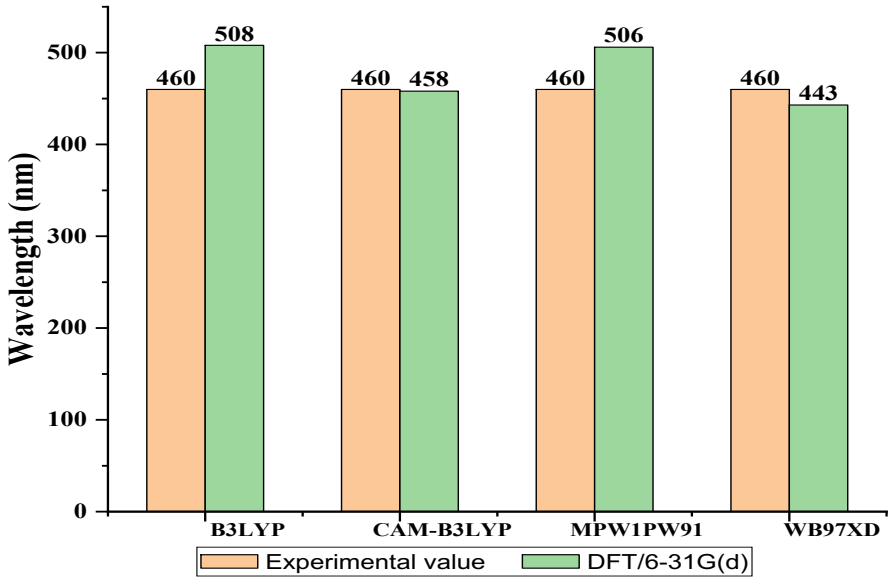

Fig7. Simulated column chart for R by B3LYP, CAM-B3LYP, MPW1PW91 and WB97XD functional at 6-31G(d)

3.3.2 Absorption spectra

The UV-visible absorption spectra of the proposed compounds (M1-M4) and the molecule R are computed at the TD-CAM-B3LYP/6-31G (d) level. Firstly, the spectrum data of absorption for all molecules in the gas phase are regrouped in **Table 4**, and illustrated in **Figure 9**. Secondly, in order to study the effect of solvation parameters on the electron excitation, the UV-visible absorption spectra of these compounds was evaluated in chloroform solvent, the spectrum data of absorption for all molecules in chloroform are listed in **Table 5**, and illustrated in **Figure 10**. In photovoltaic cell, the semi-conductor material absorbs the energy photons; this energy absorbed is inversely proportional to the wavelength by the following relation:

$$E = \frac{hc}{\lambda} \qquad \textbf{Eqn (4)}$$

h represents the Planks constant $h = 6.63 \times 10^{-34}$ J.s and c represents the speed of light $c = 3 \times 10^{8}$ m.s^{-1}

Table 4. Computed maximum absorption wavelengths (λmax, in nm), f, and major percentage contribution for all designed dyes M1 to M4 and molecule R using CAM -B3LYP/6-31G(d,p) method in the gas phase

Molecules	Calcu. λ_{max}(nm)	E_{ex} (ev)	*F*	MO/character	(%)
R	459.42	2.6987	2.2193	HOMO→LUMO	(89%)
	360.83	3.4359	1.1859	HOMO→ LUMO +1	(81%)
	348.63	3.5560	0.3317	HOMO-1→LUMO	(28%)
M1	757.53	1.6367	0.7522	HOMO→LUMO	(96%)
	453.80	2.7319	0.0447	HOMO-1→LUMO	(86%)
	393.72	3.1488	0.0009	HOMO-9→LUMO	(84%)
M2	700.20	1.7707	0.5586	HOMO→LUMO	(93%)
	528.46	2.3459	0.2249	HOMO→ LUMO +1	(93%)
	405.65	3.0562	0.0003	HOMO-12→ LUMO +1	(64%)
M3	931.10	1.3316	0.7235	HOMO→LUMO	(98%)
	486.57	2.5479	0.0164	HOMO-1→LUMO	(87%)
	407.63	3.0413	0.323	HOMO-8→LUMO	(10%)
M4	552.74	2.2431	1.5345	HOMO→LUMO	(90%)
	524.73	2.3626	0.1156	HOMO-5→LUMO	(86%)
	361.57	3.4288	0.0794	HOMO-1→LUMO	(81%

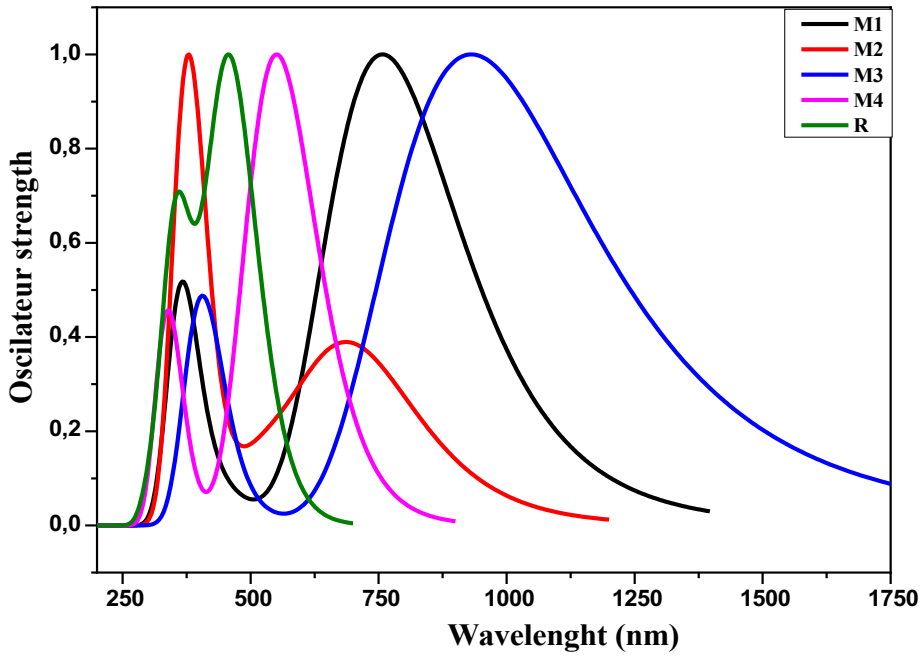

Figure 8. Absorption profile of studied compounds in the gas phase

As show in the figure 8,each molecule in the gaseous phase represents two major bands which correspond to two transitions in the absorption spectrum: $\pi \rightarrow \pi^*$ for the intense pic and $n \rightarrow \pi^*$ for the less intense peak R (λ1 = 360 nm; λ2 = 459 nm) M1 (λ1 = 371 nm; λ2 = 758 nm) M2 (λ1 = 376nm; λ2 = 700 nm) M3 (λ1 = 408 nm; λ2 = 931 nm) M4 (λ1 = 338 nm; λ2 = 553 nm). The maximum absorption wavelength of the studied compounds increases in the following order M2 (376 nm) < R (460 nm) < M4 (553 nm) < M1 (758 nm) < M3 (931), the bathochromic effect from M2 to M3 due to increase π delocalization. The strongest peak correspond to the transition from the HOMO level to the LUMO for the compounds M1, M3, M4 and R while it correspond to the transition from the HOMO-9 level to the LUMO level for the compound M2.

Table 5. Computed maximum absorption wavelengths (λmax, in nm), f, and major percentage contribution for all designed dyes M1 to M4 and molecule R using CAM -B3LYP/6-31G(d,p) method in the chloroform (solvent)

Molecules	Calcu. λ_{max}(nm)	E_{ex} (eV)	*f*	MO/character	(%)
R	473.80	2.6150	2.2000	HOMO→LUMO	(89%)
	374.13	3.3116	1.3914	HOMO →LUMO+1	(80%)
	363.70	3.4066	0.3839	HOMO→LUMO+2	(54%)
M1	758.13	1.6343	0.9682	HOMO →LUMO	(95%)
	456.33	2.7151	0.0027	HOMO-1 →LUMO	(83%)
	394.04	3.1444	0.0064	HOMO-9→LUMO	(72%)
M2	738.70	1.6772	0.5990	HOMO→LUMO	(92%)
	550.55	2.2505	0.3355	HOMO→LUMO+1	(92%)
	413.27	2.9981	0.2917	HOMO-1 →LUMO	(81%)
M3	974.26	1.2717	0.8761	HOMO →LUMO	(97%)
	499.19	2.4820	0.0003	HOMO-1 →LUMO	(86%)
	414.14	2.9918	0.3956	HOMO-2 →LUMO	(69%)
M4	598.09	2.0716	1.929	HOMO →LUMO	(94%)
	513.03	2.4151	0.000	HOMO-5 →LUMO	(93%)
	385.80	3.2115	0.000	HOMO-1 →LUMO	(81%)

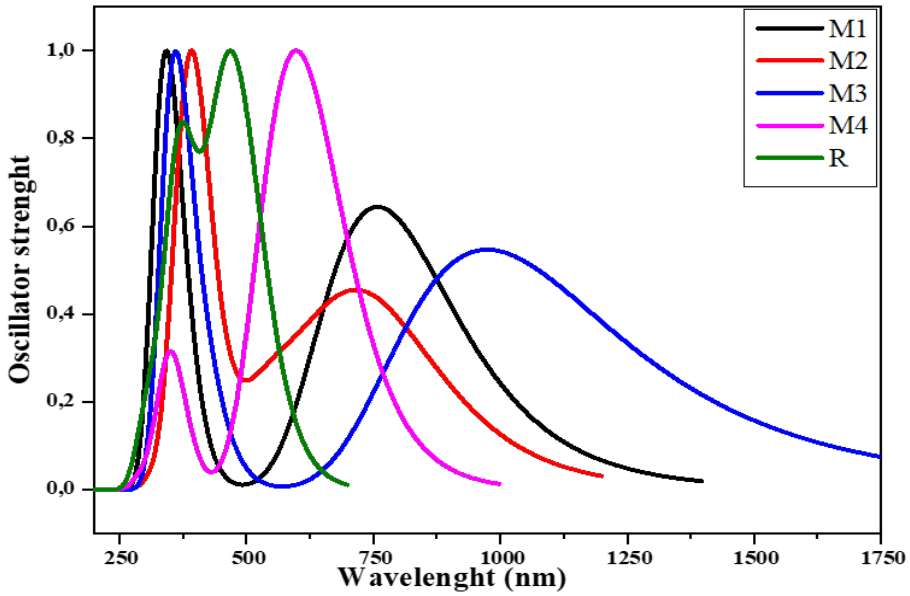

Figure 9. Absorption profile of studied compound in solvent chloroform

The solvent affected the position, the shape and the intensity of the absorption peak. Roughly, a polar solvent has a bathochromic effect on the transition $\pi \rightarrow \pi^*$; this displacement is due to a change in the stability of the molecule in its ground and excited states. As show in the figure, in the chloroform solvent, each molecule keeps these two absorption bands: R (λ1 = 360 nm; λ2 = 473.80 nm) M1 (λ1 = 371 nm; λ2 = 758 nm) M2 (λ1 = 376 nm; λ2 = 700 nm) M3 (λ1 = 408 nm; λ2 = 931 nm) M4 (λ1 = 338 nm; λ2 = 553 nm). According to the literature, the maximum band is shifted towards the higher wavelengths. The maximum wavelengths increase in the following order M2 (376 nm) < R (460 nm) < M4 (553 nm) < M1(758 nm) < M3(931). We also see a hypochromic shift on the intense peaks of the

molecules M1 and M3 caused by decrease in absorptivity as well as a Hyperchromic effect of the less intense peaks of the same compounds.

3.4 Predicting power conversion efficiency by Scharber diagram

The power conversion efficiency is one of the most critical parameters, used to compare the performance of one solar cell to another (Thul *et al*., 2009). The efficiency of a solar cell is calculated according to the following equation (Vasanthakumari *et al*., 2018):

$$PCE = \frac{(FF.V_{OC}.J_{SC})}{P_{in}} \qquad \textbf{Eqn (5)}$$

Where Pin represents the input power from the light, JSC the short-circuit current, VOC the open-circuit voltage, and FF denotes the fill factor.

The power conversion efficiency (PCE) of the donors' compounds proposed can be evaluated using the Scharber's diagram from the relationship between the band gap Eg and the $\Delta E_{LUMO} = E_{LUMO}(donors) - E_{LUMO}(acceptor)$ energy level. This model has been widely employed and approved to predict the PCE of organic solar cells combining small molecule M donor with PCBM acceptor, and it has shown that predicted PCE are in agreement with the reported experimental data (Liu *et al.,* 2014; Gim *et al*., 2016). The Scharber diagram (represented by the contour lines and colors) can be seen in **Figure 11**. The PCE of the compounds M1, M2, M3 and M4 are respectively 8,5 %, 8,2 %,10 % and 4,7 %. On the basis on obtained results, we suggest these small molecules donors for use in BHJ solar cells.

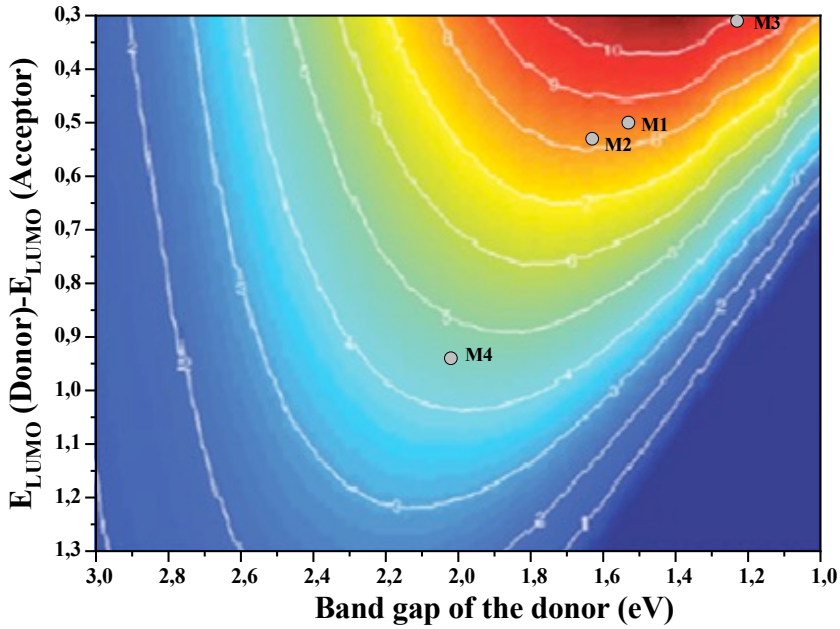

Figure 10. Prediction of PCE for donor-PC61BM cell (donor: Mi, i=1-4 and R) with Scharber diagram in chloroform solvent

3.5 Transition density matrix

The transition density matrix TDM is a tool for understanding electronic excitation processes in molecules and providing a supplemental information on the distribution of the associated electron–hole pairs as well as about the interaction between donor, acceptor and space fragments throughout the molecular skeleton interact and the movement of the charge density in the fragments, in the excited states (Taouali *et al*., 2018). TDM map allows one the identify delocalization and coherence lengths of the

electron–hole pairs: Diagonal regions represent the number of atoms contributing in transition, whereas off-diagonal zones designating the degree of coherence between the electron and the hole at different sites. Therefore, we calculated the electron hole-coherence of the first excited single state (S1) and we plotted transition density matrix map in **Figure 12**. by default, the less contribution of hydrogen atoms to the transition has been neglected (Taouali *et al*., 2018).

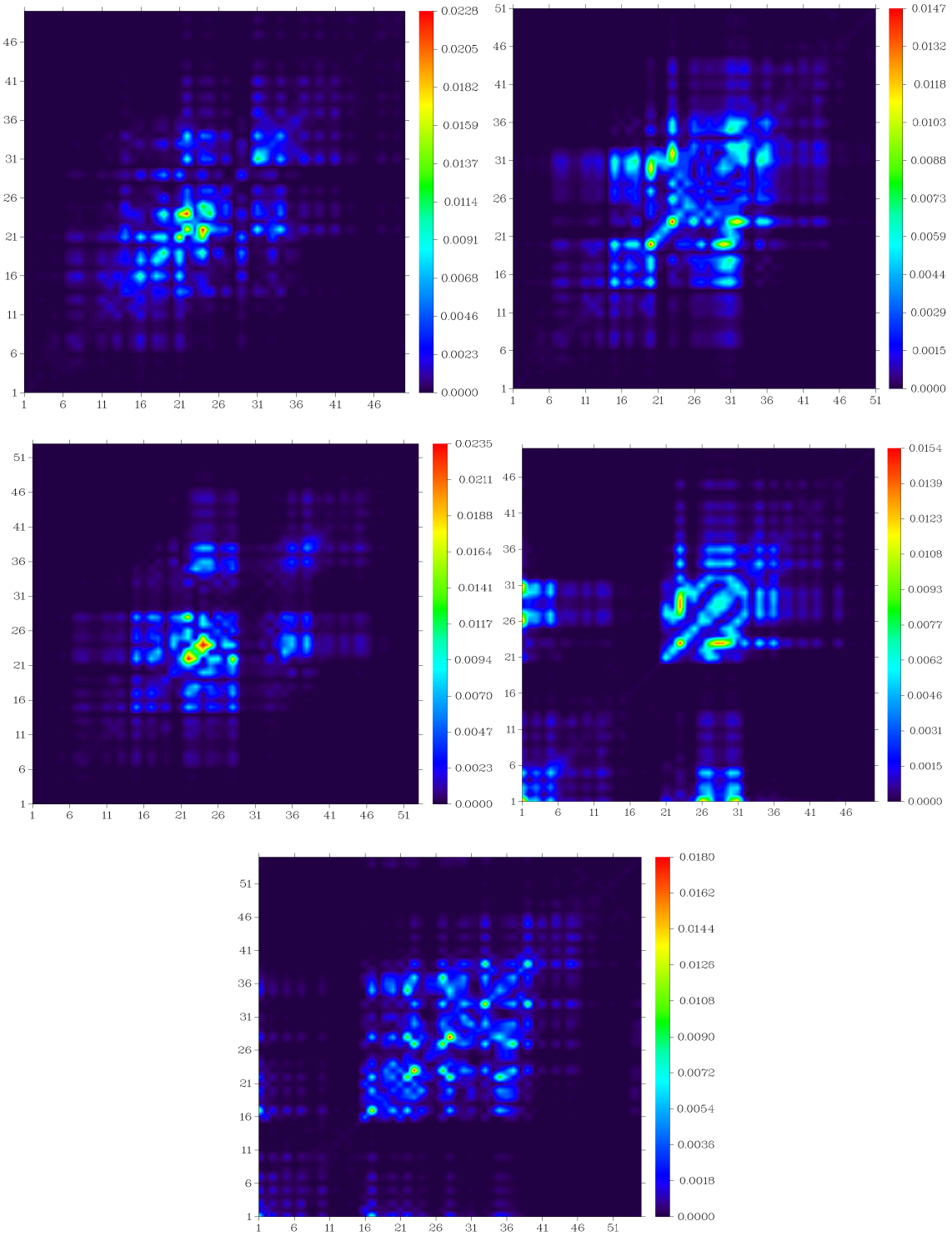

Figure 11: TDM of designed molecules (M1-M4) and R in the S1 state obtained by TD- CAMB3LYP /6-31G(d) level

When we examine the transition density matrixes map of designed molecules (Mi, I = 1-4) and R, we can observe that the electronic transition is mainly concentrated on the diagonal section, with a fixed degree of coherence between the electro and the hole around the diagonal, which indicates that charge transfer occurs along the molecular skeleton with a defined coherence length. The electronic excitations in the proposed compounds (Mi, I = 1-4) and the reference molecule R are mostly oriented diagonally, which means that the charge coherence is mainly on the donor unit, which is transferred to the acceptor via the thiophene (spacer group). The thiophene bridge facilitates the transfer of charge between the donor and the acceptor. All molecules have some charge transfer is also off diagonally. All compounds offer better charge transfer and the excitons are easier to escape the coulomb attraction.

Conclusion

In this paper, we have employed DFT and time dependent DFT (TD-DFT) computational methods to investigate the geometric, electronic, and photophysical properties of four proposed compounds have a D-π-A-π-D architecture, based on carbazole used as donor unit D, in order to determine their efficiency and use as electron donor compounds in photovoltaic cells.

- All studied compounds have quasi-planar conformation favoring the delocalization of charge intermolecular and showed smaller band gap compared to the reference molecule as well as the photovoltaic parameters Voc and αi allow the injection and transfer the electrons from suggested donor molecules to chosen acceptor (PCBM).

- The simulated UV-visible spectra of the proposed compounds represent the strong absorption in UV-visible and near infrared. In chloroform solvent, these absorptions are influenced by the bathochromic shift due to stabilization of the compounds by the polar solvent.

- The calculation of PCE by the Scharber diagrams arise the encouraging values, especially for M3, M1 and M2. Finally, the TDM analysis show the delocalization of electron transition of the donor fragment to acceptor fragment via the π-spacers group.

From these results, we note that all molecules studied can be used as electron donors in a p – n junction solar cell (BHJ), because the process of injecting electrons from the molecule to PCBM conduction band is possible.

Disclosure statement: *Conflict of Interest:* The authors declare that there are no conflicts of interest.
Compliance with Ethical Standards: This article does not contain any studies involving human or animal subjects.

References

El Alamy A., Amine A., Bouzzine S M., Hamidi M., and Bouachrine M., (2015) New Compounds Based on Quaterthiophene and Benzo [1,2,5] Thiadiazole for Solar Cells Application: Correlation Structure/Electronic Properties. *Mor. J. Chem.,* 3 (4), 688–97.

Ates M., and Uludag N., (2016) Carbazole Derivative Synthesis and Their Electropolymerization. *Journal of Solid State Electrochemistry* ., 20 (10), 2599–2612. https://doi.org/10.1007/s10008-016-3269-5.

Aydin A., and Kaya I., (2013) Syntheses of Novel Copolymers Containing Carbazole and Their Electrochromic Properties. *Journal of Electroanalytical Chemistry.,* 691 1–12. https://doi.org/10.1016/j.jelechem.2012.12.012.

Bauschlicher C W., and Partridge H., (1995) A Modification of the Gaussian-2 Approach Using Density Functional Theory. *The Journal of Chemical Physics.,* 103 (5) 1788–91.

https://doi.org/10.1063/1.469752.
Becke A D., (1993) Density-Functional Thermochemistry. III. The Role of Exact Exchange. *The Journal of Chemical Physics.,* 98 (7) 5648–52. https://doi.org/10.1063/1.464913.
Belghiti N., (2017) Matériaux Organiques π -Conjugués à Base de Thiophène , Carbazole Ou Anthracène : Synthèse , Propriètés et Modélisation. *Universite Moulay Ismail*, Meknes, Morocco 247.
Bibi S., Rasheed A., Afifa F., and Javed I., (2021) Triphenylamine Based Donor-Acceptor-Donor Type Small Molecules for Organic Solar Cells. *Computational and Theoretical Chemistry* 1198 (December 2020) 113-176. https://doi.org/10.1016/j.comptc.2021.113176.
Britel O., Fitri A., Benjelloun A.T. et al. (2022).Theoretical investigation by DFT and TDDFT the extension of π-conjugation of novel carbazole-based donor materials for bulk heterojunction organic solar cell applications. *J. Mol. Model.* 28, 351 https://doi.org/10.1007/s00894-022-05347-w
Burke D J., and Lipomi D J., (2013) Green Chemistry for Organic Solar Cells. *Energy and Environmental Science* 6 (7) 2053–66. https://doi.org/10.1039/c3ee41096j.
Chen C., (2016) Design , Synthesis and Characterization of New Organic Semi- Ecole Doctorale et Discipline Ou Spécialité. Université Toulouse 3 Paul Sabatier., 246.
Yu-ai D., Geng Y., Li H., Jin J, Wu Y., and Su Z., (2013) Theoretical Characterization and Design of Small Molecule Donor Material Containing Naphthodithiophene Central Unit for Efficient Organic Solar Cells. *Journal of Computational Chemistry.,* 34 1611–19. https://doi.org/10.1002/jcc.23298.
Duvva N., Kanaparthi R K., Kandhadi J., Marotta G., Salvatori P., De Angelis F., and Giribabu L., (2015) Carbazole-Based Sensitizers for Potential Application to Dye Sensitized Solar Cells. *Journal of Chemical Sciences.,* 127 (3) 383–94. https://doi.org/10.1007/s12039-015-0794-1.
Gambhir A., Sandwell P., and Nelson J., (2016) The Future Costs of OPV – A Bottom-up Model of Material and Manufacturing Costs with Uncertainty Analysis. *Solar Energy Materials and Solar Cells.,* 156 49–58. https://doi.org/10.1016/j.solmat.2016.05.056.
Grazulevicius J V., Strohriegl P., Pielichowski J., and Pielichowski K., (2003) Carbazole-Containing Polymers : Synthesis , Properties and Applications. *Prog. Polym. Sci.,* 28, 1297–1353. https://doi.org/10.1016/S0079-6700(03)00036-4.
Günes S., Neugebauer H., and Sariciftci N S., (2007) Conjugated Polymer-Based Organic Solar Cells. *Chemical Reviews.,* 107 (4) 1324–38. https://doi.org/10.1021/cr050149z.
Idrissi A., El Fakir Z., Atir R., Habsaoui A., Ebn Touhami M., Bouzakraoui S., (2023). Thiophene-based molecules as hole transport materials for efficient perovskite solar cells or as donors for organic solar cells, *Mater. Chem. Phys.,* 293, 126851, https://doi.org/10.1016/j.matchemphys.2022.126851
Kacimi R., Chemek M., Azaid A., Bennani M N., Alimi K., and Bejjit L., (2020) Organic Materials Based on Thiophene and Benzothiadiazole for Organic Solar Cells . Computational Investigations. *OAJ Materials and Devices.,* 5 (January) 1–11.
Kadam V S., Bhatt P A., Machhi H K., Soni S.,. Zade S S., and Patel A L., (2020) Dithienopyrrolobenzo-thiadiazole-carbazole Based D-π-A-π-D P-type Conjugated Material., *Nano Select.,* 1 (5) 491–98. https://doi.org/10.1002/nano.202000028.
Khlaifia D., Chemek M., and Alimi K., (2020) DFT/TDDFT Approach: An Incredible Success Story in Prediction of Organic Materials Properties for Photovoltaic Application,. *Mor. J. Chem.,* 8 (3) 683–99. https://doi.org/10.48317/IMIST.PRSM/morjchem-v8i3.18518
Ledwon P., (2019) Recent Advances of Donor-Acceptor Type Carbazole-Based Molecules for Light Emitting Applications., *Organic Electronics.,* 75 (June): 105422. https://doi.org/10.1016/j.orgel.2019.105422.
Liu X., Shen W., He R., Luo Y., and Li M., (2014) Strategy to Modulate the Electron-Rich Units in Donor-Acceptor Copolymers for Improvements of Organic Photovoltaics., *Journal of Physical Chemistry., C* 118 (31) 17266–78. https://doi.org/10.1021/jp503248a.
"Photovoltaics - CSIRO." n.d. Accessed March 19, 2021. https://www.csiro.au/en/research/technology-space/energy/Photovoltaics.
Politzer P., and Murray J S.. (1991) Molecular Electrostatic Potentials. In *Reviews in Computational Chemistry*,

edited by Donald B. Boyd Kenny B. Lipkowitz, Wiley-VCH, 2 : 273–312. Department of Chemistry, University of New Orleans. https://doi.org/10.1002/chin.200427290.

Vasanthakumari R., Nirmala W., Santhakumari R., Meenakshi R., Sinthiya A., (2018) Growth , Spectral , Density Functional Theory (DFT) and Hirshfeld Surface Analysis on 4-Aminopyridinium Adipate Monohydrate Nonlinear Optical Single Crystal. *Materials Science-Poland.,* 36 (2) 177–84. https://doi.org/10.1515/msp-2018-0010.

Sadiki Y A., Bouzzine S M., Bouachrine M., Hamidi M., Bejjit L., and Elhaddad M.. (2015) New Organic Compounds Based on N-Fluorene-Carbazole Moiety Fordye- Sensitized Solar Cells . Computational Study . *Mor. J. Chem.,* 1 108–21.

Govindasamy S., Govindasamy S., Prakash J., Swart H C., and Sakthivel P., (2018) Design and Chemical Engineering of Carbazole-Based Donor Small Molecules for Organic Solar Cell Applications. *Journal of Materials Science: Materials in Electronics.,* 29 (17) 14842–51. https://doi.org/10.1007/s10854-018-9621-z.

Pavel S., (2005) Loss Analysis of the Power Conversion Efficiency of Organic Bulk Heterojunction Solar Cells., *Faculté de Mathématiques et Sciences Naturelles de l'Université Carl von Ossietzky d'Oldenbourg*.,

Benjamin S., Kudla C J., Forster M., Steiger J., Anselmann R., Thiem H., and Scherf U., (2009) Amorphous Carbazole-Based (Co) Polymers for OFET Application., *Macromolecular Rapid Communications.,* 30 (14): 1258–62. https://doi.org/10.1002/marc.200900214.

Taouali W., Casida M E., Aldin A., Darghouth M H M., and Alimi K., (2018) Theoretical Design of New Small Molecules with a Low Band-Gap for Organic Solar Cell Applications: DFT and TD-DFT Study., *Computational Materials Science.,* 150 (January) 54–61. https://doi.org/10.1016/j.commatsci.2018.03.038.

Pallavi T., Gupta V P., Ram V J., and Tandon P., (2010) Spectrochimica Acta Part A : Molecular and Biomolecular Spectroscopy Structural and Spectroscopic Studies on 2-Pyranones., *Spectrochimica Acta Part A* 75: 251–60. https://doi.org/10.1016/j.saa.2009.10.020.

Barone V., Bloino J., Biczysko M., Kuno M., Caricato M., Frisch M J., and Hiscocks J., (2013) Vibrationally-Resolved Electronic Spectra in GAUSSIAN 09. *MRS Bulletin.,* 37 (02) 1–20. http://idea.sns.it/files/idea/docs/vibronic_spectra_G09-A02.pdf.

Chengjun W,, Weibin X., Linwei L., Wei L., Wang J., and Sun T., (2019) Spectroscopic Investigations and Molecular Docking Analysis of ML115: A Potential Molecular Probe of the Signal Transducer and Activator of Transcription., *Journal of Molecular Structure.,* 1175 638–47. https://doi.org/10.1016/j.molstruc.2018.08.035.

Yeongrok G., Kim D., Kyeong M., Byun S., Park Y., Kwon S., Hong S., Lansac Y., and Jang Y H., (2016) D-A-D-Type Narrow-Bandgap Small-Molecule Photovoltaic Donors: Pre-Synthesis Virtual Screening Using Density Functional Theory. *Physical Chemistry Chemical Physics.,* 18 (22) 15054–59. https://doi.org/10.1039/c5cp07536j.

Zahllou A., Abram T., Boussaidi S., Zgou2 H., Bejjit L., and Bouachrine M., (2015) Theoreticalinvestigation of New Organic Materials Based on Fluorene and Thiophene for Photovoltaic Applications., *Mor. J. Chem.,* 3: 861–71.

(2023) ; https://revues.imist.ma/index.php/morjchem/index